Available on CMS information server

CMS NOTE 2002/038

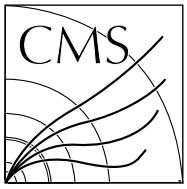

The Compact Muon Solenoid Experiment

CMS Note

Mailing address: CMS CERN, CH-1211 GENEVA 23, Switzerland

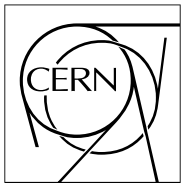

November 7, 2002

The Effect of Highly Ionising Events on the APV25 Readout Chip

R. Bainbridge, G. Hall, M. Raymond

Blackett Laboratory, Imperial College, London SW7 2AZ

R. Chierici, L. Mirabito

CERN, CH-1211 Geneva, Switzerland

Abstract

Inelastic nuclear interactions in silicon sensors can produce highly ionising particles, which in turn can generate signals equivalent of up to $\sim$1000 minimum ionising particles. These highly ionising events have been observed to cause measurable deadtime in the CMS Tracker APV25 front-end readout chip. An analysis of beam test data and a simulation of the effect in the laboratory have provided measurements of both the rate at which non-negligible deadtime is observed and the deadtime resulting from a highly ionising event. Laboratory studies also indicate that through a suitable choice of a front-end hybrid resistor, the deadtime may be reduced. The predicted inefficiency of the CMS Tracker due to highly ionising events is at the sub-percent level.

1 Highly ionising events and the deadtime mechanism

Simulation studies have shown that essentially all inelastic nuclear interactions between hadrons and silicon generate highly ionising events [1] and can result in energy depositions of up to a few hundreds of MeV in 500 μm of silicon (equivalent to $\sim$1000 minimum ionising particles). Inelastic hadronic collisions in silicon typically produce a short-range nuclear recoil ($<$ 100 μm), resulting in a highly localised energy deposition of up to a few tens of MeV, and light fragments, which can travel up to a few mm in silicon and may also be highly ionising. Events with the highest energy depositions always involve several particles. Figure 1 shows the probability of a hadronic interaction resulting in an energy deposition E_{dep} [MeV] per unit path-length in silicon for: 120 GeV pions at normal incidence in 500 μm silicon; hadrons in the CMS Tracker Inner Barrel region with their predicted energy spectra and an isotropic angular distribution, per 320 μm path-length in silicon; and hadrons in the CMS Tracker Outer Barrel region with their predicted energy spectra and an isotropic angular distribution, per 500 μm path-length in silicon. Figure 2 shows the probability of a hadronic interaction resulting in an energy deposition greater than E_{dep}, for the same hadron energy and angular distributions.

The simulation studies have also provided information on the spatial distribution of the energy depositions resulting from highly ionising events, which suggest that the bulk of the signal resulting from a highly ionising event is typically collected on one or two channels of the APV25 readout chip [2]. The magnitude of such a signal is often sufficient to saturate the preamplifier of these channels but, more importantly, the biasing scheme used to power the APV25 inverter stage provides a crosstalk path so that all 128 channels of the APV25 are affected. The bias for the inverter stage is derived from a +2.5 V (V250) supply rail via an external 100 Ω hybrid resistor, R_{inv} (see figure 3). A consequence of this biasing scheme is that a large signal at one or more of the inverter input nodes will drive down the inverter output of all the other channels. A sufficiently large signal will render all 128 channels of the APV25 insensitive to normal signals, and the duration of this insensitive state of operation is known as the deadtime. The duration of the deadtime is dependent on the magnitude of the signal generated by the highly ionising event.

2 Analysis of X5 beam test data

The effect of highly ionising events on the APV25 chip was first observed during the X5 beam test in October 2001. The aim of the test was to operate a near-final version synchronous readout system under LHC-like operating conditions. The readout system consisted of six Tracker Outer Barrel (TOB) modules, each comprising a 500 μm-thick sensor instrumented with four APV25 chips. The APV25 analogue data were delivered electrically to three FED-PMC cards [3]. The sensors were exposed to a 120 GeV pion beam with a 25 ns bunch structure similar to that used during the May 2000 beam test [4]. High instantaneous intensities, necessary for high trigger-rate conditions, were achieved by delivering pions (or muons) to the target area in trains of $\sim$50 consecutive RF buckets (spaced by 25 ns). These trains arrived repeatedly at the target area, every SPS orbit period of 23.1 μs, throughout a spill of duration $\sim$2 s. Consecutive spills were separated by a $\sim$13 s gap of no beam. Coincident signals from two scintillators, placed upstream of the sensors, identified the occupied RF buckets and provided the trigger for the readout system. The data from each triggered event were digitised and written to ZEBRA [5] files in their unsuppressed format, along with scalars identifying the run, spill, event and bunch crossing numbers. The data were analysed using ORCA [6]. Measurements of the both rate at which deadtime is observed (known as the HIP rate) and the deadtime resulting from highly ionising events, obtained from an analysis of the data taken during the X5 beam test, are presented below.

2.1 HIP rate measurements with pions and muons

If a trigger is coincident in time with the occurrence of a highly ionising event, the analogue data from the affected APV25 chip exhibit large (and often truncated) signals in several channels and a negative shift from the nominal 'baseline' analogue level in all other channels. If the energy deposition is sufficiently large then the output of all channels (not seeing the large signal) is driven to the lower limit of the APV25 dynamic range. Consequently, all further signals from minimum ionising particles, along with the usual pedestal structure observed across the 128 channels, are suppressed, resulting in deadtime. Figure 4 shows an example of a highly ionising event. The output of one APV25 in the third module exhibits a cluster of adjacent strips containing large signals and a shifted baseline. A high level of activity is observed in the modules downstream.

The common mode (CM) level, a slow time-varying signal common to all channels of an APV25 and manifest in the data as a deviation from the nominal 'baseline' analogue levels, was calculated from the analogue data read out from each APV25 chip for each triggered event. The CM distribution is shown in figure 5. Increasingly

Run	N_{trig}	N_{hip}	$\langle N_{\pi/\mu} \rangle$	N_{plane}	R_{hip}
20730 (π)	244986	955	1.9	5	$(4.1 \pm 0.1) \cdot 10^{-4}$
20655 (π)	215938	858	2.0	5	$(4.0 \pm 0.1) \cdot 10^{-4}$
20670 (μ)	225000	7	1.9	5	$(3.3 \pm 1.2) \cdot 10^{-6}$

Table 1: HIP rate measurements, R_{hip} [per bunch crossing per particle per 500 μm of silicon], for incident pions and muons (quoted with the statistical error).

large energy depositions from highly ionising events result in increasingly shifted baselines and therefore a tail at negative CM values. The pronounced peak found at the end of the tail is due to the limited dynamic range of the APV25, which provides an upper limit on the maximum observable shift from the nominal baseline level. Negative CM levels can also result from triggering a short time after the occurrence of a highly ionising event, when the baseline may be returning to its nominal position during the APV25 'recovery'. The tail at positive CM levels results from baselines overshooting their nominal position during this 'recovery' period.

A collection of adjacent strips exhibiting a signal-to-noise ratio greater than some threshold value are identified as a 'cluster' of strips containing signal. Figure 6 shows a 2-dimensional plot of cluster size [strips] versus cluster signal [ADC counts] for clusters found in data frames with CM $<$ -140 ADC counts (i.e, with baselines very near the lower limit of the available dynamic range). In data frames with large negative CM level, two types of cluster can be clearly identified: those produced by minimum ionising particles, which typically contain signals of $\sim$100 ADC counts in one or two strips; and those produced by highly ionising particles, which typically contain signals of up to several thousand ADC counts spread across several strips. It is these large signals which are responsible for the observed baseline shifts. The magnitude and spatial distribution of the energy depositions in the silicon sensors cannot be deduced from the analogue data, as signals are frequently truncated due to the limited dynamic range of the APV25 and inter-strip capacitive coupling of the sensors effectively 'smears' any observed signal over an increased number of channels.

Due to the characteristic response of the APV25, highly ionising events that result in non-negligible deadtime can be identified in the data by imposing thresholds on the common mode, CM, and the cluster signal, Q_{clu}:

$$\begin{aligned} \text{CM} &\leq -140 \quad \text{[ADC counts]} \\ Q_{clu} &\geq +300 \quad \text{[ADC counts]} \end{aligned} \tag{1}$$

The HIP rate, defined to be the rate at which deadtime is observed [per bunch crossing per particle per 500 μm of silicon][1)], is calculated by normalising the number of highly ionising events, N_{hip}, by the factor ($N_{trig} \cdot \langle N_{\pi/\mu} \rangle \cdot N_{plane}$), where N_{hip} highly ionising events are observed in N_{trig} triggered events, $\langle N_{\pi/\mu} \rangle$ is the mean pion (or muon) multiplicity and N_{plane} is the number of sensors used to collect the data. Table 1 summarises the numbers used to calculate the HIP rate from the data runs 20730 and 20655 (pion beam) and run 20670 (muon beam). The HIP rate, for 120 GeV pions traversing a 500 μm silicon sensor, is observed to be $\sim 4 \cdot 10^{-4}$ [per bunch crossing per pion per 500 μm of silicon]. As muons cannot interact hadronically, collisions between muons and silicon nuclei rarely generate the largest energy depositions, resulting in a negligible HIP rate measurement.

2.2 Deadtime measurement with pions

'Disabled' APV25 chips, which are experiencing deadtime after a highly ionising event, are also identifiable in the data, as the APV25 data frames contain baselines shifted to the lower limit of the available dynamic range and no signal in any of the 128 channels. Furthermore, the pedestal structure normally observed across the 128 channels is also suppressed. This is clearly seen in figure 7, which shows the distribution of the peak-to-peak spread observed in the 128 analogue values of APV25 data frames. The peak at $<$ 5 ADC counts is a consequence of data frames containing fully suppressed baselines with no signal or pedestal structure. Typically, pedestal structure and the presence of signals result in a minimum peak-to-peak spread of $\sim$15 ADC counts. Therefore, disabled APV25 chips are identified by imposing thresholds on the common mode, CM, and the spread in the raw analogue data, δ:

$$\begin{aligned} \text{CM} &\leq -140 \quad \text{[ADC counts]} \\ \delta &\leq +10 \quad \text{[ADC counts]} \end{aligned} \tag{2}$$

[1)] The thickness of the sensor in a TOB module is 500 μm.

Deadtime cannot be directly measured on an event-by-event basis with the X5 data (where 'event' here means a highly ionising event) but, by taking advantage of the X5 beam structure and understanding the temporal distribution of triggers during data taking, it was realised that an 'event-averaged' measurement of the deadtime was possible. A measurement of the deadtime can be made by considering how the probability of observing a disabled APV25 in the analogue data from triggered events depends on the trigger position within the bunch trains.

The bunch crossing (BX) number appended to the analogue data from each triggered event provides the time stamp for that event and allows the structure of the X5 beam to be investigated by considering the distribution of triggers in time. The BX data clearly exhibit modularity 924, which is interpreted as an SPS orbit containing 924 RF buckets and therefore having an orbit period of 23.1 μs. Figure 8 shows the distribution of triggers during a single spill (extraction) of pions during run 20655. The BX number is plotted along the abscissa and the position in the SPS orbit of the occupied RF bucket providing the trigger (given by BX modulo 924) is plotted along the ordinate. It can be seen that triggers are confined to RF bucket numbers $\sim$20 to $\sim$70, reflecting the delivery of trains of $\sim$50 consecutive bunches to the target area.

Coincident signals from two scintillators, placed upstream of the detectors, identified the occupied RF buckets within a train and resulted in a trigger being issued to the readout system. For high trigger-rate studies, triggers were issued to the readout chain only if a particular combination of occupied and empty RF buckets was observed. During run 20655, the required combination of occupied (labelled as '1') and empty (labelled as '0') RF buckets was '1001', resulting in two triggers, spaced by 75 ns, being distributed to the readout system (this is the minimum separation of triggers accepted by the APV25 chip [7]). Requiring this particular combination of occupied and empty RF buckets resulted in an approximately uniform distribution of triggers throughout the bunch trains. The temporal distribution of triggers within bunch trains is shown in figure 9. Triggers are taken from multiple spills for increased statistics.

Figure 10 shows the number of highly ionising events and disabled APV25 chips identified in the data from triggered events as a function of trigger position, during run 20655 (pion beam). The difference in statistics between the two distributions is due to the increased probability of observing a disabled APV25 due to the non-zero deadtime. Normalising these two distributions to the distribution of triggers observed during run 20655 (see figure 9) provides the probability of observing a highly ionising event or disabled APV25 per triggered event as a function of trigger position, as shown in figures 11 (a) and (b), respectively.

As seen in figure 11 (a), the probability of observing a highly ionising event per triggered event is constant at $\sim 4 \cdot 10^{-3}$ during the bunch train and zero before and after. Normalising this probability to the number of 500 μm sensor planes (5) and the mean pion multiplicity (1.9) observing during run 20655 provides a HIP rate measurement of $\sim 4 \cdot 10^{-4}$ per bunch crossing per pion per 500 μm silicon, which is in good agreement with the HIP rate measurements listed in table 1.

The probability of observing a disabled APV25 depends on the probability of a highly ionising event occurring in one of the preceding occupied RF buckets of the train. Importantly, trains (of duration $\sim$1.25 μs) arrive at the target area every SPS orbit period (23.1 μs) and so are sufficiently spaced such that highly ionising events occurring in one train cannot contribute to any deadtime observed in the following train. Therefore, the probability of observing a disabled APV25 is zero at the beginning of a train (as there are no preceding occupied RF buckets). This probability increases as the trigger position moves further into the train, due to the increasing probability of observing a highly ionising event, and then saturates. Saturation occurs because only highly ionising events that precede a trigger by a time interval less than the induced deadtime can contribute to the probability of observing a disabled APV25. The time taken for the probability to saturate provides an 'event-averaged' measurement of the deadtime. Figure 11 (b) shows the probability of observing a disabled APV25 as a function of trigger position. The deadtime, obtained from the time taken for the probability to saturate, is measured to be 325 ± 50 ns (equivalent to 13 ± 2 bunch crossing intervals) for the criteria described above that were used to identify highly ionising events and disabled chips.

3 Simulating highly ionising events in the laboratory

Highly ionising events were simulated in the laboratory by injecting large (known) signals directly into a number of channels of the APV25 chip, via the input pads on the front-end of the chip. Adjacent channels of the APV25 were coupled to these large signals through a capacitor network to simulate inter-strip capacitive coupling. After each simulated highly ionising event, a signal equivalent to 3-MIPs traversing 500 μm of silicon was then injected into a different APV25 channel and the APV25 triggered a latency period later to read out the amplitude of the APV25 output for that channel. Measurements were repeated for different delays between the signal injection

N_{chans}	R_{inv} [Ω]	α [ns]	β [ns/MeV]	E_{thr} [MeV]	τ [MeV]
2	100	255	0.87	7.3	0.6
2	50	155	0.00	11.9	44.5
1	100	127	0.07	11.9	9.2
1	50	76	0.40	18.9	6.7

Table 2: Summary of fit parameters used to parameterise the dependence of the measured deadtime on the simulated energy deposition, for various values of R_{inv} and N_{chans} (the number of channels on which signal was injected).

times (up to 5 μs, in 0.1 μs steps) to obtain the amplitude of the APV25 output as a function of time after the simulated highly ionising event. The behaviour of the baseline as a function of time after a highly ionising event was obtained by repeating these series of measurements without the injection of the 3-MIP signal. Examples of the resulting temporal traces, with and without the injection of the 3-MIP signal, are shown in figure 12 (a). The response of the APV25 to the 3-MIP signal as a function of time after a highly ionising event is provided by the difference between the two traces, as shown in figure 12 (b). These response traces were obtained for a range of simulated energy depositions, 5 to 100 MeV, with the signal injected either on one or shared between two channels, as shown in figure 13. The measured deadtime was defined to be the time interval for which zero signal amplitude was observed.

Figure 14 shows the measured deadtime as a function of the simulated energy deposition for signal injected on two APV25 channels, with both the nominal hybrid resistor value, R_{inv} = 100 Ω and a reduced resistor value, R_{inv} = 50 Ω. The same is shown in figure 15 for signal injected on a single APV25 channel. The simulated energy deposition is accurate to $\pm 5\%$ (this error is largely attributable to the non-negligible tolerance of the charge injection capacitors) and the deadtime measurement (obtained from the response curves in figure 13) is accurate to ± 5 ns. The dependence of the measured deadtime on the simulated energy deposition can be parameterised with the following equation:

$$\Gamma(E_{dep}) \;=\; \begin{cases} \left(\alpha \,+\, \beta \cdot E_{dep}\right) \cdot \left(1 \,-\, exp\left\{\frac{-(E_{dep} - E_{thr})}{\tau}\right\}\right) & E_{dep} \,>\, E_{thr} \\ 0 & E_{dep} \,\leq\, E_{thr} \end{cases} \tag{3}$$

where $\Gamma(E_{dep})$ [ns] is the deadtime resulting from an energy deposition E_{dep} [MeV], E_{thr} [MeV] is the threshold energy deposition required for non-negligible deadtime to be observed, τ [MeV] characterises the initial exponential dependence, and the following linear rise is characterised by the constants α [ns] and β [ns/MeV]. The best fits to the deadtime measurements are represented by dashed lines in figures 14 and 15, and the values of the fit parameters are summarised in table 2.

Figures 14 and 15 show that the observed deadtime for a given energy deposition is sensitive to both the number of APV25 channels on which the signal is collected and the resistor value, R_{inv}. It can be seen that the deadtime is reduced by decreasing the value of the external resistor, R_{inv}. For the case when signal is collected on two APV25 channels, the maximum observed deadtime is reduced from $\sim$350 ns to $\sim$100 ns when R_{inv} is reduced from 100 Ω to 50 Ω. Furthermore, the threshold energy deposition (E_{thr}) required for deadtime to be observed is increased from $\sim$7 MeV to $\sim$12 MeV. When signal is collected on a single APV25 channel, the maximum observed deadtime is $\sim$150 ns.

The cumulative energy deposition probability spectra shown in figure 2 can be used in conjunction with the laboratory-measured energy deposition thresholds to predict the probability of a hadronic interaction in silicon resulting in deadtime. For a threshold energy deposition of 7 MeV (for the case when the signal generated by a highly ionising event is collected on two APV25 channels and R_{inv} = 100 Ω), the probability of observing an energy deposition greater than 7 MeV is $\sim 8 \cdot 10^{-4}$ for 120 GeV pions incident on 500 μm of silicon, which is in agreement with the experimentally measured HIP rate at X5, as listed in table 1. Similarly, predictions can be made for the CMS TIB and TOB regions. In the TIB region, the predicted probability of observing an energy deposition greater than 7 MeV is $\sim 5 \cdot 10^{-4}$ per hadron per 320 μm of silicon. With a reduced resistor value of R_{inv} = 50 Ω and therefore an increased energy threshold of E_{thr} = 12 MeV, the probability is reduced to $\sim 3 \cdot 10^{-4}$ per hadron per 320 μm of silicon. In the TOB region, the corresponding probabilities are $\sim 6 \cdot 10^{-4}$ and $\sim 4 \cdot 10^{-4}$ per hadron per 500 μm of silicon.

R_{inv} [Ω]	Inefficiency [10^{-3}]		
	X5 (500 μm)	TIB (320 μm)	TOB (500 μm)
100	1.04	0.52	0.72
50	-	0.03	0.05

Table 3: Inefficiency, ε_{tot} [per % occupancy per unit path-length in silicon], predicted for the X5 and CMS TIB and TOB environments, with signal shared between two APV25 channels and resistor values R_{inv} = 100 Ω and R_{inv} = 50 Ω.

4 Inefficiency due to highly ionising events

As discussed above, deadtime in the APV25 caused by highly ionising events can result in the loss of signal. For a given energy deposition, E_{dep} [MeV], in a silicon sensor, the predicted inefficiency, $\varepsilon(E_{dep})$ [per % occupancy per unit path-length in silicon], is given by the equation:

$$\varepsilon(E_{dep}) \;=\; \Phi(E_{dep}) \cdot \frac{\Gamma(E_{dep})}{25\ [\mathrm{ns}]} \cdot \eta \cdot 128 \quad ; \quad \varepsilon_{tot} \;=\; \sum_{E_{dep}} \varepsilon(E_{dep}) \tag{4}$$

where $\Phi(E_{dep})$ is the probability of a hadronic interaction in silicon resulting in an energy deposition E_{dep}, $\Gamma(E_{dep})$ [ns] is the deadtime resulting from an energy deposition E_{dep}, η [%] is the occupancy and the factor 128 accounts for all 128 channels of an APV25 being disabled. The probability, $\Phi(E_{dep})$, of an energy deposition E_{dep} is provided by figure 1, which shows the differential energy deposition probability spectra for hadronic interactions in silicon with incident hadrons of various energy and angular distributions. The corresponding deadtime, $\Gamma(E_{dep})$, is provided by the fits to the laboratory measurements obtained with the signal injected on two APV25 channels and resistor values R_{inv} = 100 Ω and 50 Ω (see figure 14).

The resulting inefficiency, $\varepsilon(E_{dep})$, as a function of energy deposition, E_{dep}, is shown in figure 16 for both the CMS TIB and TOB environments. It can be seen that the predicted inefficiency resulting from a given energy deposition is reduced for R_{inv} = 50 Ω. The inefficiency distribution predicted for 120 GeV pions at normal incidence (as during the X5 beam test) is also plotted for comparison.

The total inefficiency, ε_{tot}, is obtained by summing $\varepsilon(E_{dep})$ over all energy depositions, E_{dep}, and table 2 summarises the total inefficiencies [per % occupancy per unit path-length in silicon] expected for both the X5 and CMS TIB and TOB environments. The quoted inefficiencies for the TIB and TOB regions are for the unit path-lengths of 320 μm and 500 μm, respectively. For a hybrid resistor value of R_{inv} = 100 Ω, the predicted inefficiency is $\sim$ 0.7%, which is reduced by an order of magnitude to $\sim$ 0.05% for R_{inv} = 50 Ω.

5 Conclusions

Highly ionising events in silicon sensors can cause measurable deadtime in the APV25 readout chip. For extremely large signals, $\gg$100 minimum ionising particles, all 128 channels of the chip are affected, due to the design of the biasing for the APV25 inverter stage.

The effect of highly ionising events on the APV25 has been studied with analysis of data from the X5 beam test and in the laboratory. All results obtained from these studies and from a simulation of π-Si interactions in silicon [1] are in good agreement. The rate at which deadtime is observed is $< 10^{-3}$ and the deadtime resulting from highly ionising events is measured to be $\sim$300 ns. Laboratory measurements also indicate that deadtime for a given energy deposition may be reduced by decreasing the value of a front-end hybrid resistor.

The inefficiency due to highly ionising events, per % occupancy per unit path-length, has been predicted for the CMS environment, using results from simulation and laboratory measurements, and is calculated to be at the sub-percent level.

6 Acknowledgements

The authors would like to thank all involved in the October 2001 X5 beam test but the following persons are particularly noteworthy for their important work on the DAQ, trigger, slow control, environmental control and detector systems; F. Drouhin, P. Gras, N. Marinelli, J. C. Reyna, P. Siegrist, A. Tsirou and P. G. Verdini. The authors would also like to thank the UK Particle Physics and Astronomy Research Council for their financial support of his work.

7 Glossary

MIP	Minimum Ionising Particle
HIP	Highly Ionising Particle
TIB	Tracker Inner Barrel
TOB	Tracker Outer Barrel
FED-PMC	Front End Driver - PCI Mezzanine Card
V125	+1.25 Voltage rail
V250	+2.50 Voltage rail
V_{SS}	Ground

References

[1] M. Huhtinen, *Highly ionising events in silicon detectors*, CMS Note 2002/011, March 2002

[2] L. L. Jones et al., *The APV25 Deep Submicron Readout Chip for CMS Detectors*, Proceedings of the 5th Workshop on Electronics for LHC experiments, September 1999

[3] J. Coughlan et al., *A PMC based ADC card for CMS Tracker readout*, Proceedings of the 5th Workshop on Electronics for LHC experiments, September 1999

[4] M. Bozzo et al., *Observation of the slow-extracted 25 ns bunched beam*, Proceedings of Chamonix XI, January 2001

[5] *The ZEBRA system*, CERN Program Library Long Writeups Q100/Q101, February 1995

[6] *The TriDAS Project*, Technical Design Report, volume 2: Data Acquisition and High Level Trigger, CERN/LHCC 02-XX (in preparation)

[7] L. L. Jones, *APV25 User-Guide Manual, version 2.2*, September 2001

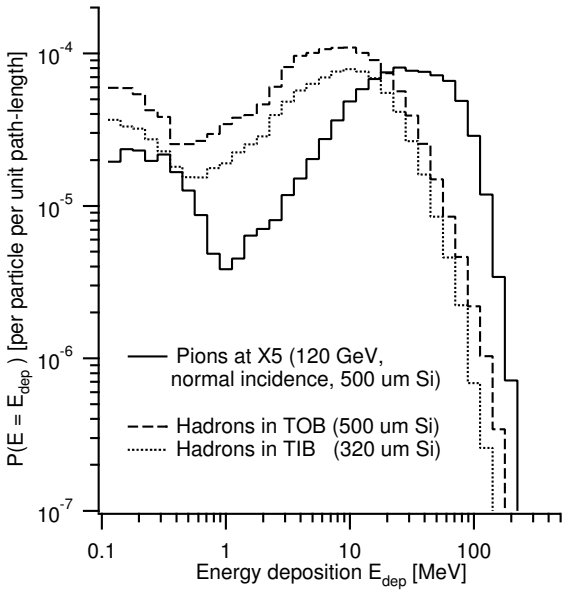

Figure 1: Differential energy deposition probability spectra, providing the probability of a hadronic interaction in silicon resulting in an energy deposition E_{dep} [MeV] per unit path-length in silicon for: 120 GeV pions at normal incidence in 500 μm silicon; hadrons in the CMS Tracker Inner Barrel region with their predicted energy spectra and an isotropic angular distribution per 320 μm path-length in silicon; and hadrons in the CMS Tracker Outer Barrel region with their predicted energy spectra and an isotropic angular distribution per 500 μm path-length in silicon. Taken from [1].

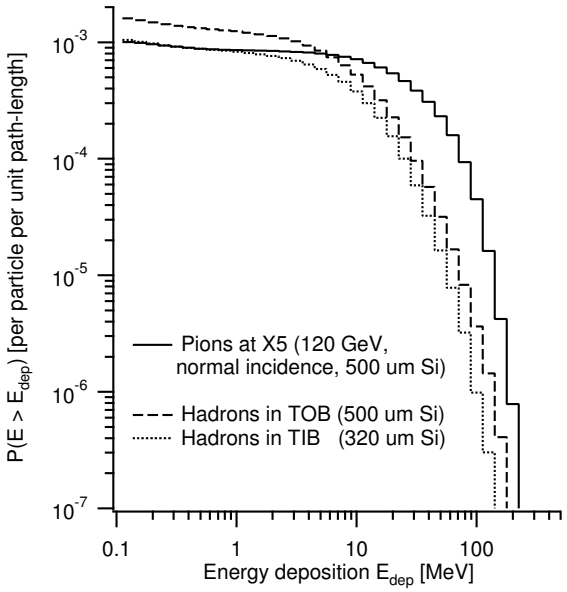

Figure 2: Cumulative energy deposition probability spectra, providing the probability of a hadronic interaction in silicon resulting in an energy deposition greater than E_{dep} [MeV] per unit path-length in silicon for: 120 GeV pions at normal incidence in 500 μm silicon; hadrons in the CMS Tracker Inner Barrel region with their predicted energy spectra and an isotropic angular distribution per 320 μm path-length in silicon; and hadrons in the CMS Tracker Outer Barrel region with their predicted energy spectra and an isotropic angular distribution per 500 μm path-length in silicon. Taken from [1].

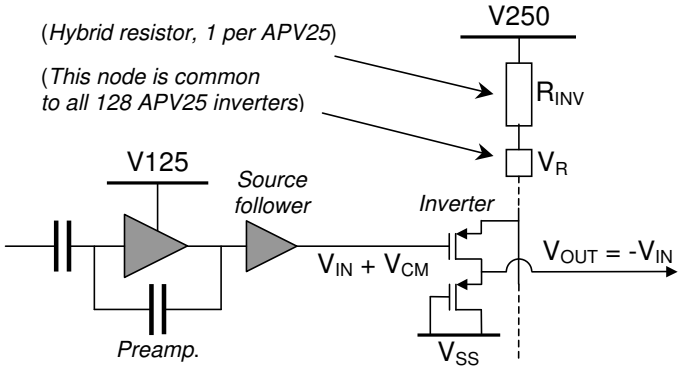

Figure 3: Schematic of the front-end amplifying stages of a single APV25 channel. The biasing for the inverter stage is derived from the $+2.50\ V$ (V250) supply via an external hybrid resistor, R_{inv}. There is one resistor per APV25 chip.

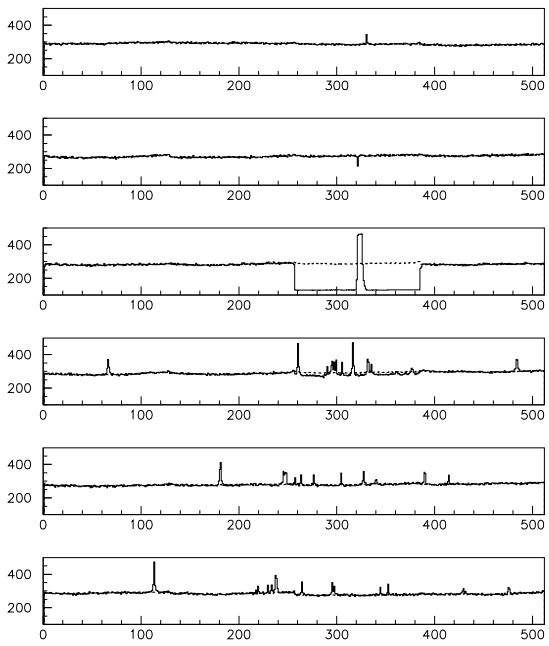

Figure 4: Raw analogue data from 6 modules displaying a highly ionising event. The output of one APV25 chip exhibits a cluster of adjacent strips containing large signals and a negative shift in all other channels.

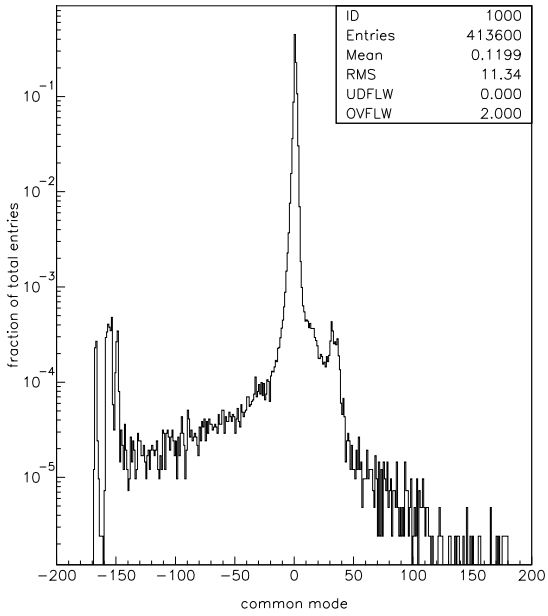

Figure 5: Distribution of common mode levels [ADC counts]. The long tail and pronounced peak at negative CM values result from data frames containing shifted baselines.

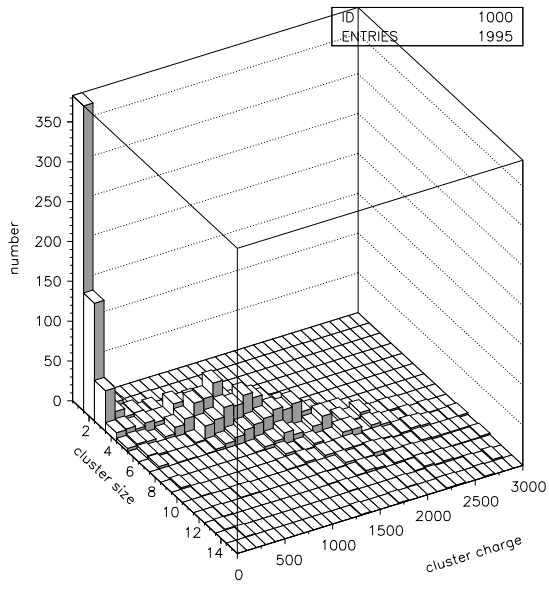

Figure 6: Cluster size [strips] versus cluster signal [ADC counts], for clusters found in data frames with CM < -140 ADC counts. Two types of cluster are distinguishable, those resulting from minimum ionising particles and those from highly ionising events.

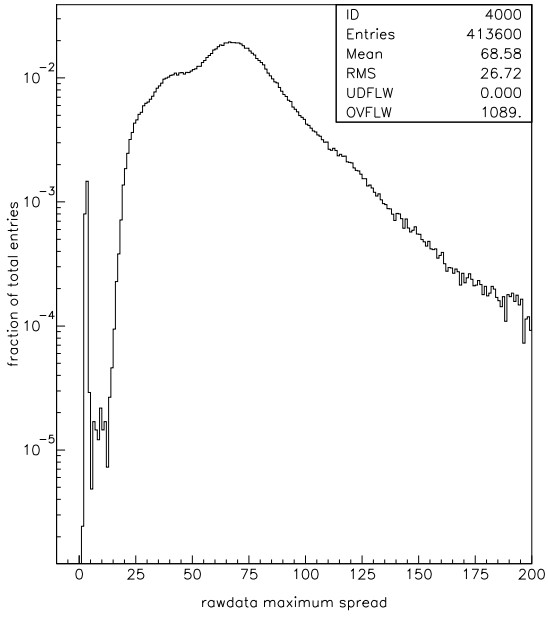

Figure 7: Peak-to-peak spread [ADC counts] in the raw analogue data of the 128 channels from an APV25 chip. The peak at < 5 ADC counts is due to APV25 chips that have collected a signal sufficiently large to result in deadtime, i.e, all further signals and the pedestal structure are suppressed.

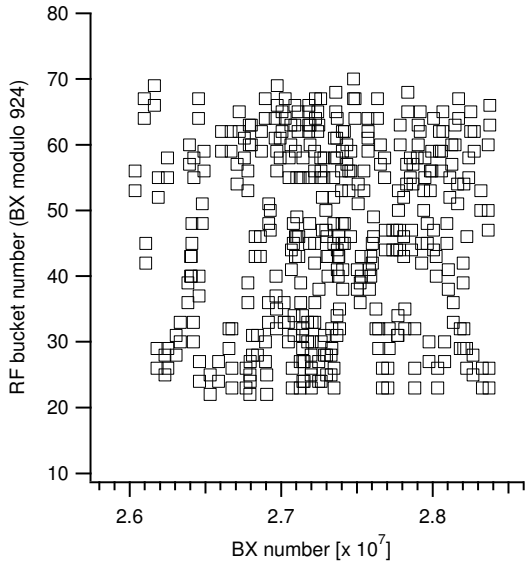

Figure 8: Temporal distribution of triggers in a single spill (extraction) from run 20655. Triggers are confined to certain RF bucket numbers (see ordinate) due to the finite length of the bunch trains.

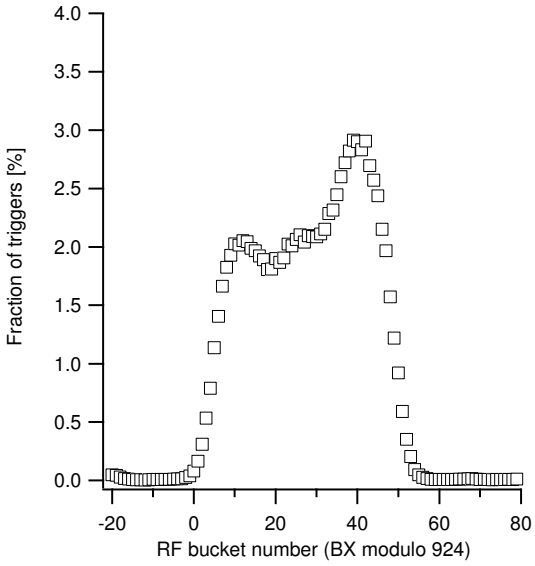

Figure 9: Temporal distribution of triggered events within bunch trains, for run 20655.

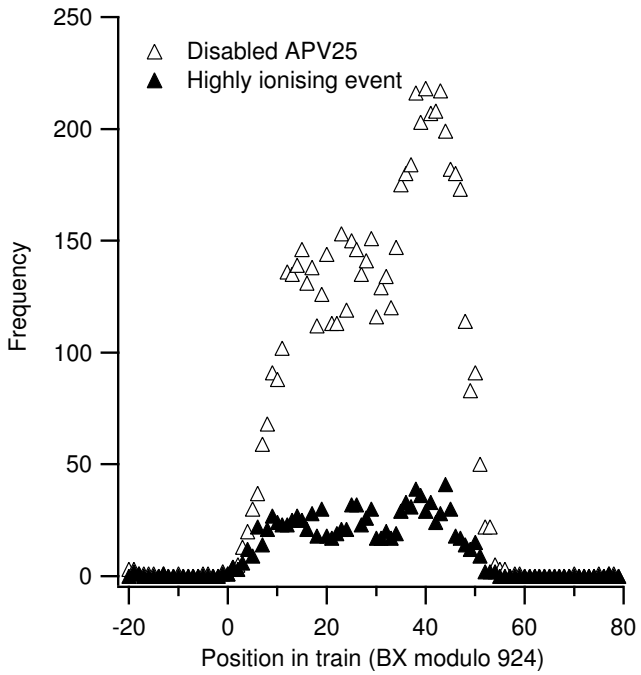

Figure 10: Number of highly ionising events (closed triangles) and disabled APV25 chips (open triangles) identified in the data as a function of trigger position, for run 20655.

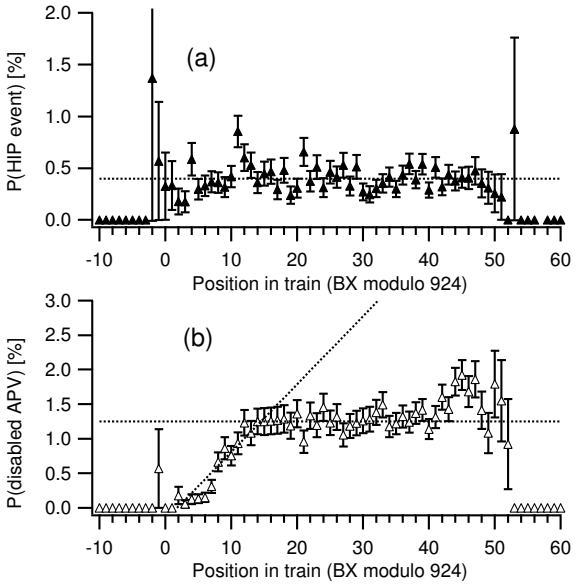

Figure 11: Probability of observing, (a) a highly ionising event, (b) a disabled APV25, as a function of trigger position. The probability of observing a highly ionising event is independent of trigger position within the bunch train, whereas the probability of observing a disabled APV25 saturates after some time. This provides a measurement of the deadtime resulting from highly ionising events.

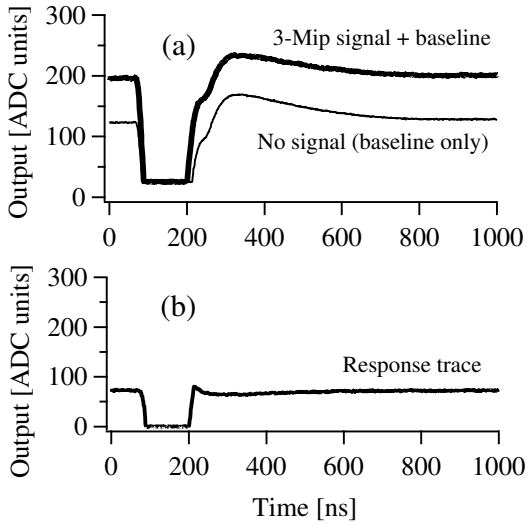

Figure 12: The traces in (a) show the output of a single APV25 channel versus time after a simulated HIP event (injected at ∼70 ns), for a 3-MIP signal injection and no signal injection (baseline only). The difference between the two traces is shown in (b), which provides the response trace of the APV25 to the 3-MIP signal.

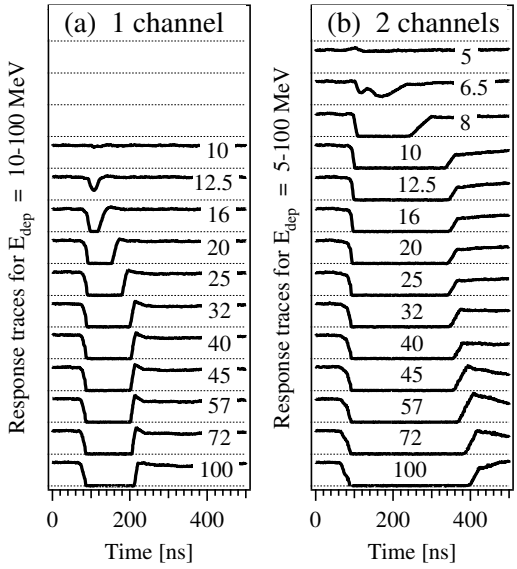

Figure 13: The response of the APV25 to a 3-MIP signal after the injection of a HIP-like signal, ranging in magnitude from 5 to 100 MeV, on (a) one APV25 channel or, (b) shared between two channels. Measurements performed with R_{inv} = 100 Ω.

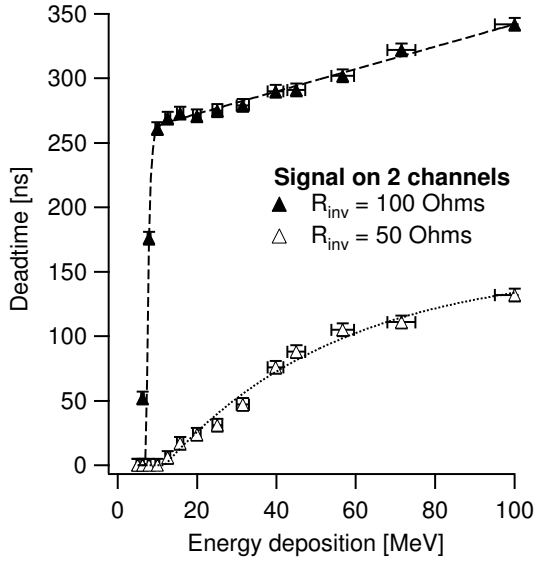

Figure 14: Deadtime as a function of simulated energy deposition for signal injected on two APV25 channels, with R_{inv} = 100 Ω (closed triangles) or R_{inv} = 50 Ω (open triangles). The dashed lines show fits to the data (see table 2 and equation 3).

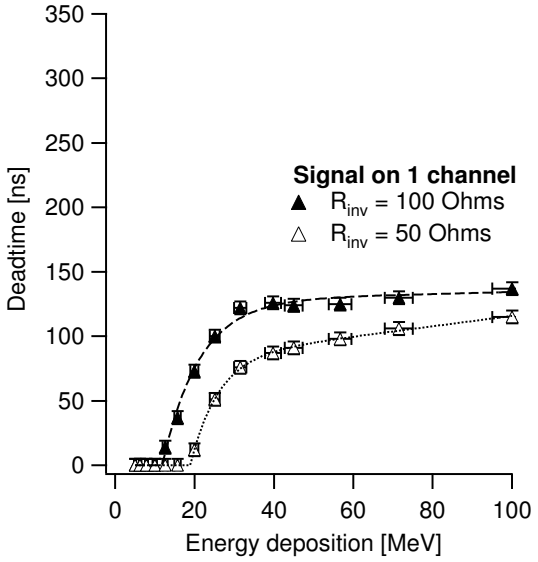

Figure 15: Deadtime as a function of simulated energy deposition for signal injected on one APV25 channel, with R_{inv} = 100 Ω (closed triangles) or R_{inv} = 50 Ω (open triangles). The dashed lines show fits to the data (see table 2 and equation 3).

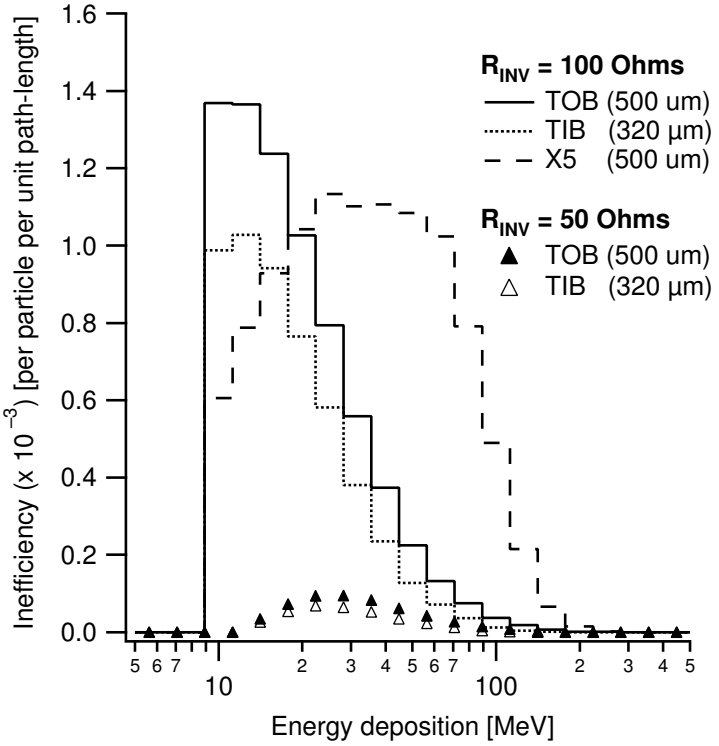

Figure 16: Inefficiency, $\varepsilon(E_{dep})$ [per % occupancy per unit path-length in silicon] as a function of energy deposition E_{dep} [MeV] for various values of R_{inv} and: 120 GeV pions at normal incidence in 500 μm silicon (as during the X5 beam test); hadrons in the CMS Tracker Inner Barrel region with their predicted energy spectra and an isotropic angular distribution per 320 μm path-length in silicon; and hadrons in the CMS Tracker Outer Barrel region with their predicted energy spectra and an isotropic angular distribution per 500 μm path-length in silicon .